Scientia Iranica B (2015) 22(6), 2142–2149

SCIENTIA IRANICA

Sharif University of Technology
Scientia Iranica
Transactions B: Mechanical Engineering
www.scientiairanica.com

Evaluation of shear behavior of deep beams with shear reinforced with GFRP plate

M.S. Kim[a], H. Kim[a], H. Park[a], N. Ahn[b] and Y.H. Lee[a,*]

a. *Department of Architectural Engineering, Kyung Hee University, 1732, Deogyeong-daero, Giheung-gu, Yongin-si, Gyeonggi-do, 446-701, Korea.*
b. *Department of Architectural Engineering, Sejong University, 209, Neungdong-ro, Gwangjin-gu, Seoul, 143-747, Korea.*

Received 22 May 2014; received in revised form 10 May 2015; accepted 10 August 2015

KEYWORDS
Glass fiber reinforced polymer;
Deep beam;
Strut-and-tie model;
Shear strength;
Shear reinforcement.

Abstract. To evaluate the shear performance of deep beams reinforced with Glass Fiber Reinforced Polymer (GFRP) plate, a test was conducted on 8 specimens. Test variables included reinforcement, shear span ratio, area of reinforcement, and effective depth. The effects of the test parameters on the shear strength of the test specimens were evaluated. The test result showed that smaller span ratio leads to larger shear strength, and that increase in the area of reinforcement and effective length increased shear strength. All test results were compared with strut-and-tie models suggested by ACI 318 and CSA.

1. Introduction

Because FRP materials have advantages, such as high-strength-to-weight ratio, corrosion resistance, and easy handling; they have been introduced as a substitute for steel reinforcement. Several studies have been conducted using sheet or bar type FRP as reinforcement [1-3]. The hear performance and bending test results of slender beams with FRP reinforcing bars are already sufficiently provided. There is also a design process proposed with this type in ACI 440.1R-06 [4], CSA S806-02 [5], and JSCE-97 [6]. However, research using FRP as shear reinforcement was conducted restrictively [7,8]. An earlier paper proposed easily fabricated plate type shear reinforcement considering the brittle characteristics of FRP [9]. Kim et al. [9] performed a shear test on a slender beam embedded with GFRP plate reinforcement to examine the shear performance. However, unlike slender beams, non-linear strain distribution is nominal in deep beams. The direct compression strut formed between the loading point and support tends to increase shear strength. This created a distinctive failure mode compared to slender beams. In deep beams, shear reinforcement controls the concrete strut and increases load-carrying capacity. Therefore, an increase in shear performance is expected by applying the high tensile strength of FRP shear reinforcement in deep beams. To verify the performance of the proposed shear reinforcement, this paper aims to experimentally investigate the shear performance of GFRP plate shear reinforced deep beams. Also the strut-and-tie modeling approach used in the steel reinforcement was examined to see its validity for deep beam shear reinforced with GFRP plate.

*. *Corresponding author. Tel.: +82-31-201-2864; Fax: +82-31-202-8854*
E-mail addresses: kimminsook@khu.ac.kr (M.S. Kim); 2kimhc@khu.ac.kr (H. Kim); parkhaeun@khu.ac.kr (H. Park); nsahn@sejong.ac.kr (N. Ahn); leeyh@khu.ac.kr (Y.H. Lee)

2. Experimental program

2.1. Material properties

The properties of the materials used in the experiment are listed in Table 1. The design strength of the concrete used is 45 MPa. Compressive strength was tested

Table 1. Material properties of steels and GFRP plate.

	Diameter (mm)	Area (mm^2)	Tensile strength (MPa)	Modulus of elasticity (GPa)
Tensile reinforcement	25.4	506.7	500	200
GFRP	-	-	480	50

after 28 days and the average strength was 44.6 MPa. The yield strength of the tensile reinforcement was 500 MPa, and steel reinforcement with a diameter of 25 mm was used. GFRP plate with an opening was used as shear reinforcement. As shown in Figure 1, horizontal and vertical components cross each other at right angles. The total width and height of the plates are expressed as b_f and h_f, respectively.

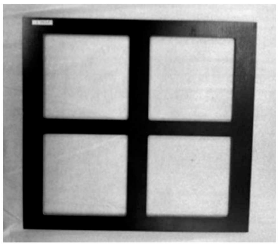
(a) Shape of GFRP

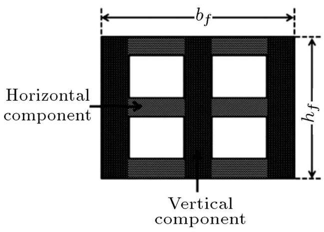

(b) Dimension of GFRP

Figure 1. GFRP Plate.

2.2. Specimen details

Seven specimens reinforced with GFRP plate and 1 specimen without shear reinforcement were fabricated. The main parameters for the experiment are: span-to-depth ratio (a/d), reinforcement area (A_f), and effective depth (d). Arrangements of the control specimen and GFRP plate reinforced specimens are shown in Figure 2. The total length of the specimen is 2800 mm and the clear span length is 1800 mm. The width of the section is 300 mm, and the height of each one is 450 mm, 500 mm, and 550 mm, respectively. Effective depth (d) is 370 mm, 420 mm, and 470 mm

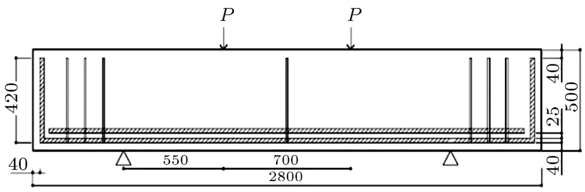

(a) M-2

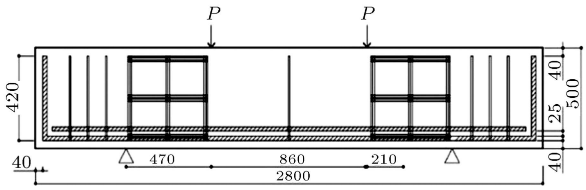

(b) GAM-1

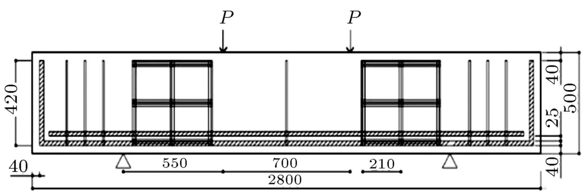

(c) GAM-2

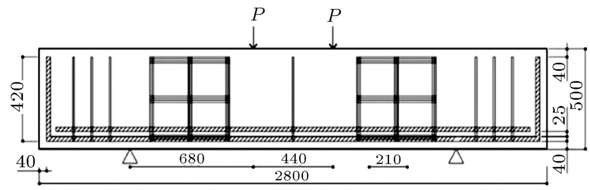

(d) GAM-3

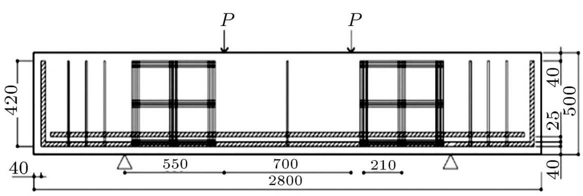

(e) GBM-2

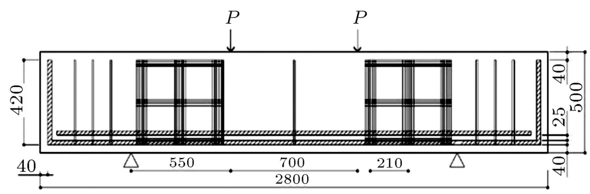

(f) GCM-2

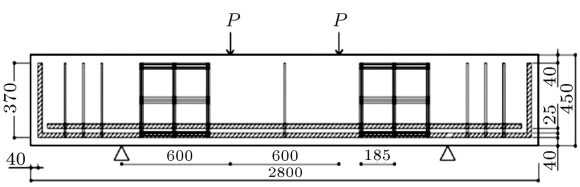

(g) GAS-3

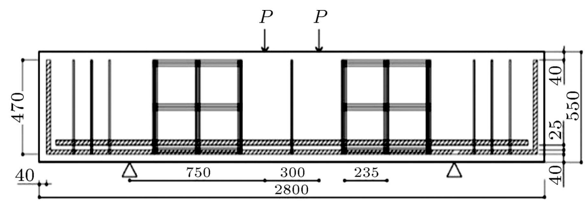

(h) GAL-3

Figure 2. Arrangement of GFRP plates in the specimen.

Table 2. Specimen details.

Specimen	a/d	b	d	FRP Shear reinforcement				
				Type of shear reinforcement	Width (mm)	Thickness (mm)	Reinforcement area (mm^2)	Distance between adjacent FRP plates (mm)
M-2	1.3	300	420	-	-	-	-	-
GAM-1	1.1	300	420	GFRP	20	1.5	120	210
GAM-2	1.3	300	420	GFRP	20	1.5	120	210
GAM-3	1.6	300	420	GFRP	20	1.5	120	210
GBM-2	1.3	300	420	GFRP	40	1.5	240	210
GCM-2	1.3	300	420	GFRP	60	1.5	360	210
GAS-3	1.6	300	370	GFRP	20	1.5	120	185
GAL-3	1.6	300	470	GFRP	20	1.5	120	235

GAM-1

***G*=Shear reinforcements**
G: Deep beam reinforced of GFRP plate
M: Control deep beam

***A*=Shear reinforcement area**
A: 120 mm^2
B: 240 mm^2
C: 360 mm^2

***M*=Effective depth**
S: 370 mm
M: 420 mm
L: 470 mm

1=Span-to-depth ratio
1: 1.1
2: 1.3
3: 1.6

Figure 3. Notation to indicate the type of each specimen.

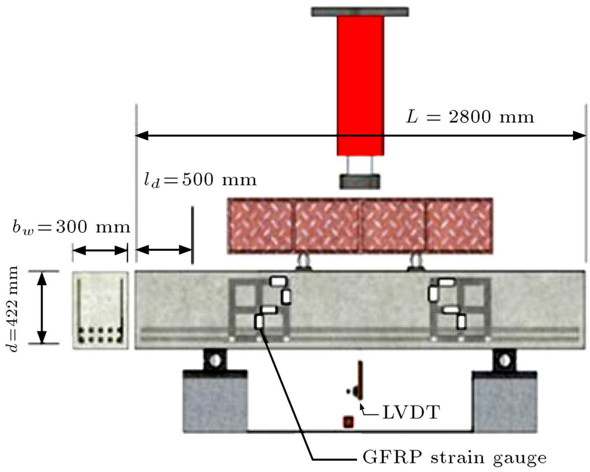

Figure 4. Specimens setting and strain gauge.

each. From the loading point, a 500 mm embedment length is designed on both sides. The cover thickness is 40 mm. Span to depth ratio is 1.1, 1.3, and 1.6. The notation to identify each specimen is shown in Figure 3. All details of the specimens are listed in Table 2.

2.3. *Test setup*

A load was applied to each specimen at a rate of 5 kN/min using a hydraulic jack with maximum capacity of 5,000 kN (Figure 4). The force generated by the hydraulic jack was transmitted to the center of the steel spreader beam, which was installed to apply a two-point loading to the beam specimen. The magnitude of the loading was measured by a load cell attached to the bottom of the jack. A Linear Variable-Differential Transducer (LVDT) was installed at the bottom center of the specimen to measure vertical displacement. Distances between the two-loading points were adjusted according to shear span-to-depth ratio. To measure the strain of the GFRP plate, a strain gauge was installed in the vertical and horizontal strips of the plate. Specifics of the test setup and gauge point are shown in Figure 4.

3. Strut-and-tie model

3.1. *ACI 318*

The deep beam is classified as a Disturbed region (D-region) in which localized stress concentration occurs. The general concept cannot be applied to the D-region. Since its span-to-depth ratio is small, it is supported with arch action. According to [10], a steel reinforced deep beam should be calculated using the Strut-and-Tie Model (STM). In this study, the design strength of the specimens is calculated by the STM of ACI 318-11. STM consists of compression components (struts), tension components (ties), and the intersection of such components (nodes). Strut represents compressive force in concrete, ties represents tension in steel, and nodes represent the point in a joint where the axes of the struts, ties, and concentrated forces are acting on the joint intersection. Struts have main compressive force in the main direction. As shown in Eq. (1), the nominal strength of a concrete strut (F_{ns}) is a multiple of effective compressive force (f_{ce}) and the area of concrete (A_{ce}). The area of the strut is the width of the member times the width of the strut, and effective compressive force can be calculated by Eq. (2).

$$F_{ns} = f_{ce} A_{cs}, \tag{1}$$

$$f_{ce} = \nu f'_c, \tag{2}$$

$$f_{ce} = 0.85 \beta_s f'_c. \tag{3}$$

The effective strength coefficient (ν) used in Eq. (2) can be calculated with the effective coefficient (β_s) in Eq. (3). When the area is constant, 1.0 is used as β_s. When a bottle shape strut meets reinforcement criteria, 0.75 is used. When it does not meet criteria, 0.6λ is used. The criteria for using 0.75 or 0.60λ can only be used when reinforcement for resisting the strut's horizontal tensile strength and compression strength is crossed. The decrease in the confinement stress of the strut, caused by tensile force, can be solved by transverse reinforcement. The center line of the strut and transverse reinforcement should cross each other. In this case, 0.75 or 0.6 is used as the coefficient constant. Also, the tensile member and tensile flange of the member use 0.4. In all other cases, 0.6 is used. λ is determined according to concrete type. Normal concrete is 1.0, sand lightweight concrete is 0.85 and lightweight concrete is 0.75.

3.2. CSA A23.3

In ACI 318, the strength reduction factor used in the calculation of the strength of the strut is determined by geometry conditions and concrete types. On the other hand, CSA A23.3 [11] indicates the strength of the strut as a function of tensile strain and the angle between the strut and tie. In addition, CSA A23.3 limits the maximum compressive stress in a concrete strut to 85% of the compressive strength (f'_c). Effective compressive stress (f_{cu}) is given in Eq. (4). The principal tensile strain (ε_1) crossing the inclined concrete strut is expressed in Eq. (5).

$$f_{cu} = \frac{f'_c}{0.8 + 170\varepsilon_1}, \tag{4}$$

$$\varepsilon_1 = \varepsilon_s + (\varepsilon_s + 0.002)\cot^2\theta_s, \tag{5}$$

where θ_s is the angle between the strut and tie, and the tensile strain of reinforcement (ε_s) is assumed to be 50% of the yield strain of 0.002.

4. Test results

4.1. Cracking and failure mode

In the beginning, flexural cracks occurred at the tension zone in the middle of the spans. After initial flexural cracks, vertical cracks also appeared in the shear span-to-depth. It tends to move towards the loading point as the load increases. The point sustains both bending and shear. In the beginning, the bending strength is dominant in the shear span-to-depth. However, shear strength is dominant as the load increases. The beam with a ratio of less than 2.5 also fractures due to diagonal crack. However, in addition to diagonal crack, fracture in the loading point from the high compressive force of the compression strut in the loading point and resistance point occurs simultaneously. Figure 5(a) shows the failure behavior of the specimen with ratio 1.1, and Figure 5(b) and (c) show the failure behavior of specimens with ratios 1.3 and 1.6. As in Figure 5, shear compressive failure occurred in specimens with ratios 1.1 to 1.6.

(a) GAM-1 ($a/d = 1.1$)

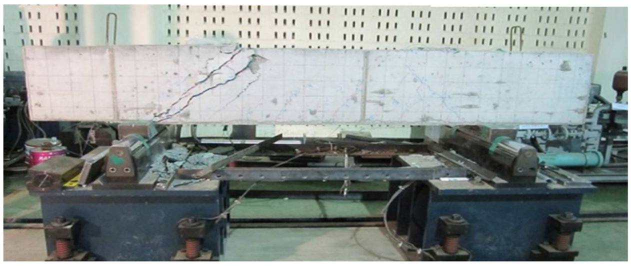

(b) GAM-2 ($a/d = 1.3$)

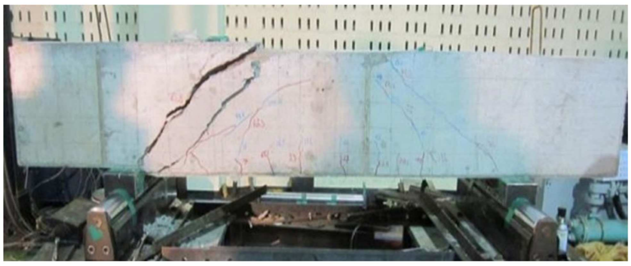

(c) GAM-3 ($a/d = 1.6$)

Figure 5. Cracking and failure mode.

4.2. Shear reinforcement

To evaluate the contribution of GFRP plate reinforcement in shear strength, the load-deflection curve of a non-reinforced specimen (M-2) and a GFRP plate reinforced specimen (GAM-2) is shown in Figure 6. Except for reinforcement, all other factors were controlled to be exactly the same. M-2 and GAM-2 both showed similar behavior before occurring shear crack. However, they showed a difference in stiffness afterwards. It seems

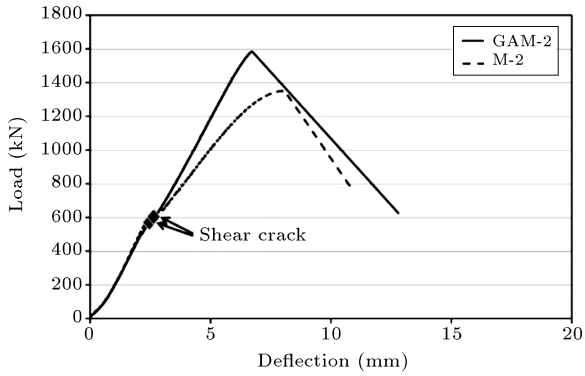

Figure 6. Load-deflection curves (shear reinforcement).

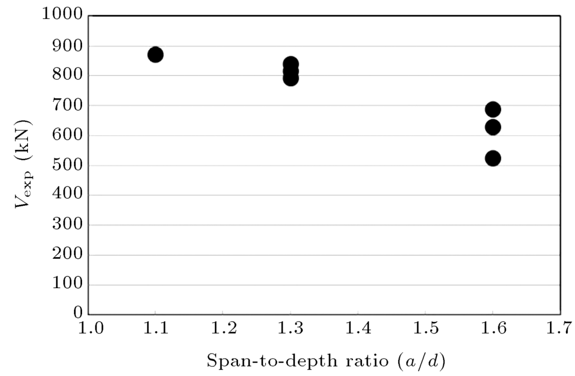

Figure 7. Experimental shear strength values depending on the span-to-depth ratio.

that the resistance of GFRP plate to crack leads to high shear performance. The maximum loading of GAM-2 was 1580 kN and that of M-2 was 1350 kN. This shows a 230 kN increase in shear strength by reinforcing with the GFRP plate.

4.3. Span-to-depth ratio

Figure 7 shows the shear strength of specimens reinforced with GFRP plate, with span-to-depth ratios of 1.1, 1.3, and 1.6 each. The maximum load increased as the span-to-depth ratio decreased. This is, as shown in Table 3, because the angle between the inclined strut and the horizontal tie increases as the ratio decreases.

Table 3. Summary of the test results.

Specimens	**Span-to-depth ratio (a/d)**	**Degree (°)**	**Strut width**	**V_{exp} (kN)**
GAM-1	1.1	35.41	146.33	871.67
GAM-2	1.3	31.28	141.07	792.60
GAM-3	1.6	26.34	133.81	628.85
GBM-2	1.3	31.28	141.07	816.09
GCM-2	1.3	31.28	141.07	839.68
GAS-3	1.6	25.34	132.23	524.51
GAL-3	1.6	26.82	134.56	688.68

The increase in angle decreases proportionally to the load in the strut, and increases the width of the strut at the same time. In other words, when the span-to-depth ratio is small, the maximum load increases because the change in width is more influential than the load.

4.4. Shear reinforcement area

ACI 318-11 regulates the minimum shear reinforcement area in deep beams, as shown in Eqs. (6) and (7). The GFRP plate in this study is designed based on these equations. As in Table 2, 120 mm^2 is the minimum shear reinforcement area and 240 mm^2 is twice the minimum shear reinforcement area. An area of 360 mm^2 is three times that of the minimum shear reinforcement area. With different area specimens, the difference in the shear performance of different area types was determined.

$$A_v \geq 0.0025 b_w s, \qquad s \leq \begin{cases} \frac{d}{5} \\ 300 \text{ mm} \end{cases} \tag{6}$$

$$A_{vh} \geq 0.0025 b_w s_2, \qquad s_2 \leq \begin{cases} \frac{d}{5} \\ 300 \text{ mm} \end{cases} \tag{7}$$

To analyze the characteristics of each specimen, the load-deflection curves of specimens GAM-2, GBM-2 and GCM-2 are shown in Figure 8. As expected, as the area increased, maximum load increased. As shown in Figure 9, compared to M-2, GAM-2 is 17.1% higher, GBM-2 is 20.5% higher and GCM-2 is 24.0% higher. The experiment verified that the loading increased as the shear reinforcement increased.

4.5. Effective depth

Effective depth is an important factor determining the flexure and shear performance of a concrete member. In general, the member can bear more load if the effective depth is longer. The shear strengths of specimens GAS-3, GAM-3, GAL-3, each with effective depth 370 mm, 420 mm, and 470 mm, are compared in Figure 10. The result showed that loading increased

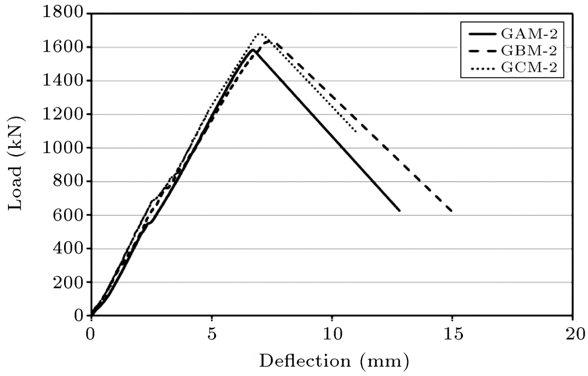

Figure 8. Load-deflection curves (shear reinforcement area).

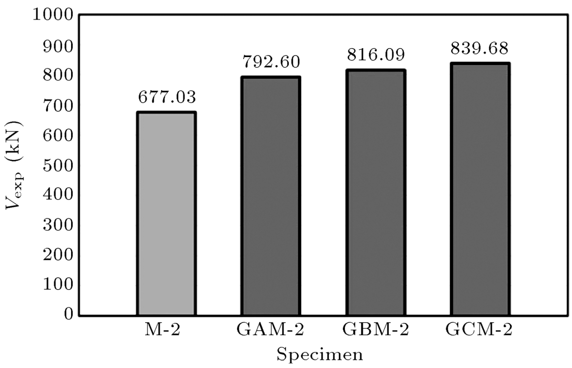

Figure 9. Effect of the shear reinforcement area.

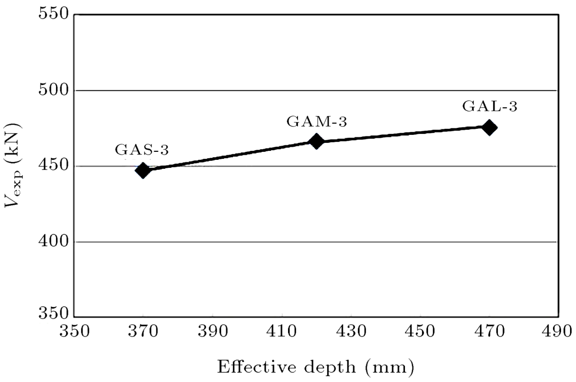

Figure 10. Effect of the effective depth on shear strength.

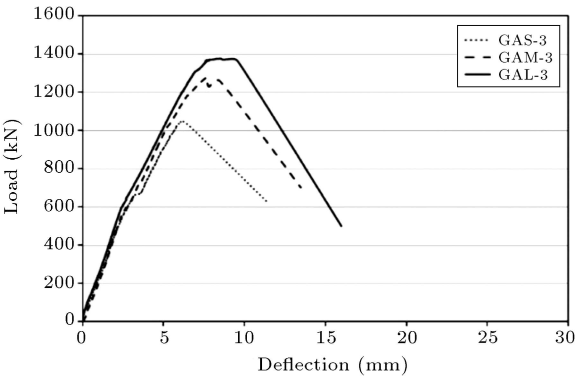

Figure 11. Load-deflection curves (effective depth).

as the effective depth increased. The load-deflection curve, according to effective depth, is shown in Figure 11. In the same load, GAS-3 showed the highest deflection followed by GAM-3 and GAL-3, sequentially. Also, maximum loading tends to increase in order. GAL-3 can stand 1380 kN, GAM-3 can stand 1250 kN and GAS-3 can stand 1050 kN. It shows that the specimens' maximum loading increased and deflection decreased as the effective depth increased. This is because the internal force of the strut increases as the area of the strut increases. The area of the strut increases as the area of the member and amount of reinforcement increase, which can be achieved with longer effective depth.

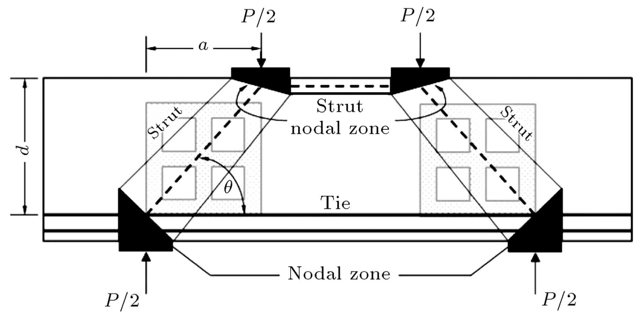

Figure 12. Strut-tie model of the GFRP plate reinforced deep beams.

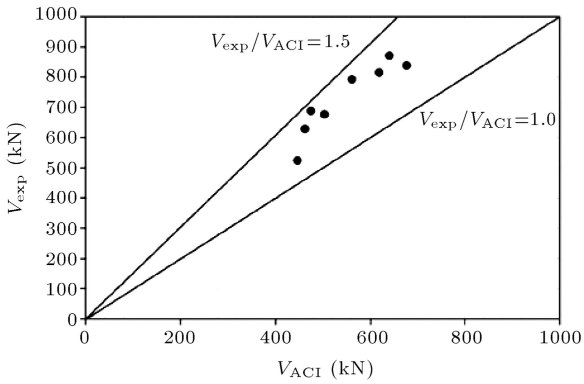

Figure 13. Ratios of the test results to the ACI 318 STM predictions on shear strength.

4.6. Comparison of experimental results and predictions by STM

To evaluate the applicability of STM in deep beams reinforced with GFRP plate, the design shear strength of the specimen and experimental results were compared. As shown in Figure 12, STM consists of struts, ties, and nodes. Table 4, together with Figures 12 and 13 compare the test results with shear strength using strut-and-tie models from ACI and CSA. The STM approaches of ACI 318 and CSA A23.3 were generally conservative. From Table 4, the mean value of the shear strength ratio ($V_{\mathrm{exp}}/V_{\mathrm{ACI}}$) is 1.33, with a standard deviation of 0.10 in ACI 318-11, and the shear strength ratios ($V_{\mathrm{exp}}/V_{\mathrm{cal}}$) were between 1.0 and 1.5, as shown in Figure 13. The STM of CSA A23.3 gives a mean value of 1.68 and a deviation of 0.25. The shear strength ratios ($V_{\mathrm{exp}}/V_{\mathrm{CSA}}$) were between 1.4 and 2.1, as shown in Figure 14. While the shear strength ratio is 1.37 in the specimen with a shear span-to-depth ratio of 1.1, the shear strength ratio is 1.99 in the specimen with a shear span-to-depth ratio of 1.6. The conservatism of STM in CSA decreases as shear span-to-depth ratio decreases because of the use of large tensile strains in calculating the capacities of the diagonal struts. The reduction of angle (θ_s) between the strut and tie, due to the increase in shear span-to-depth ratio, leads to increased tensile strain. Therefore, the effective compressive strength is reduced.

Table 4. Comparison of test results with predictions of ACI and CSA.

Specimens	V_{exp} (kN)	V_{ACI} (kN)	V_{CSA} (kN)	V_{exp}/V_{ACI}	V_{exp}/V_{CSA}
M-2	677.03	504.34	420.56	1.34	1.61
GAM-1	871.67	641.40	636.10	1.36	1.37
GAM-2	792.60	561.94	478.16	1.41	1.66
GAM-3	628.85	466.37	315.64	1.35	1.99
GBM-2	816.09	619.54	535.76	1.32	1.52
GCM-2	839.68	677.14	593.36	1.24	1.48
GAS-3	524.51	447.30	293.19	1.17	1.79
GAL-3	688.68	475.55	333.92	1.45	2.06
Average	-	-	-	1.33	1.68
Standard deviation	-	-	-	0.09	0.25

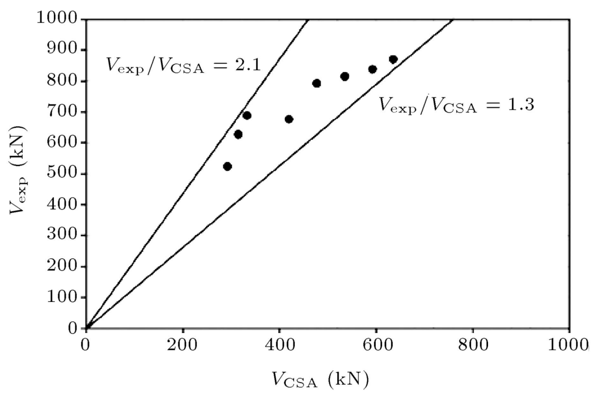

Figure 14. Ratios of the test results to the CSA A23.3 STM predictions on shear strength.

5. Conclusions

To study the shear performance and behavior of deep beams reinforced with GFRP plate, experiments were undertaken using the following factors: different materials, shear span-to-depth ratios, areas and effective depth. The STM in ACI318-11 and CSA A23.3 were used to compare the experimental results with analytical shear strengths.

As the shear span-to-depth ratio of the test specimen decreases, the maximum shear strength increases. This is because the increase in cross sectional area from the increase in strut width influences shear performance more than a decrease in applied loading. From the variable shear reinforcement area, shear performance tends to increase as the area of the GFRP plate increases. From the variable effective depth, maximum load increased and deflection minimized as the effective depth increased, as expected. In the comparison, the STM approaches of both ACI 318 and CSA A23.3 yielded generally conservative results. The ACI code gave a mean value of 1.33 with a standard deviation of 0.09. The Canadian code showed a mean value of 1.48 with a standard deviation of 0.27. Therefore, it was determined that the strut-and-tie model in ACI 318-11 was applicable to the GFRP plate reinforced concrete deep beam as its shear strength prediction.

Nomenclature

A_{ce}	Cross-sectional area at one end of a strut in a strutd-and-tie model, taken perpendicular to the axis of the strut (mm^2)
A_{cs}	Area of concrete strut (mm^2)
A_v	Area of shear reinforcement within spacing s (mm^2)
A_{vh}	Area of shear reinforcement parallel to flexural tension reinforcement within spacing s_2 (mm^2)
b_w	Web width (mm)
d	Distance from extreme compression fiber to centroid of longitudinal tension reinforcement (mm)
f'_c	Specified compressive strength of concrete (MPa)
f_{ce}	Effective compressive strength of the concrete in a strut or a nodal zone (MPa)
f_{cu}	Limiting compressive strength of the concrete (MPa)
F_{ns}	Nominal strength of a strut (kN)
s	Center-to-center spacing of items, such as longitudinal reinforcement, transverse reinforcement (mm)
s_2	Center-to-center spacing of longitudinal shear or torsion reinforcement (mm)

β_s Factor to account for the effect of cracking and confining reinforcement on the effective compressive strength of the concrete in a strut

ε_s Tensile strain in the concrete in the direction of the tension tie

ν Strength coefficient

Acknowledgments

This work was supported by the National Research Foundation of Korea (NRF) using a grant funded by the Korean government (MSIP) (NRF-2011-0016332).

References

1. El-Salakawy, E. and Benmokrane, B. "Serviceability of concrete bridge deck slabs reinforced with fiber-reinforced polymer composite bars", *ACI Structural Journal*, **101**(5), pp. 727-736 (2004).
2. Chen, J.F. and Teng, J.G. "Shear capacity of FRP-strengthened RC beams: FRP debonding", *Construction and Building Materials*, **17**(1), pp. 27-41 (2003).
3. Rahimi, H. and Hutchinson, A. "Concrete beams strengthened with externally bonded FRP plates", *Journal of Composites for Construction*, **5**(1), pp. 44-56 (2001).
4. ACI Committee 440.1R-06. *Guide for The Design and Construction Concrete Reinforced with FRP Bars (ACI 440.1R-06)*, p. 42, American Concrete Institute, Farmington Hills, USA (2006).
5. CAN/CSA-S806-02. *Design and Construction of Building Components with Fiber Reinforced Polymers (CSA-S806-02)*, p. 177, Canadian Standards Association, Mississauga, ON, Canada (2002).
6. JSCE, *Recommendations for Design and Construction of Concrete Structures Using Continuous Fiber Reinforced Materials*, p. 325, Japan Society of Civil Engineer, Tokyo, Japan (1997).
7. El-Sayed, K., El-Salakawy, E. and Benmokrane, B. "Mechanical and structural characterization of new carbon FRP stirrups for concrete members", *Journal of Composites for Construction*, **11**(4), pp. 352-362 (2007).
8. Sundarraja, M.C. and Rajamohan, S. "Strengthening of RC beams in shear using GFRP inclined strips-an experimental study", *Construction and Building Materials*, **23**(2), pp. 856-864 (2009).
9. Kim, D.J., Kim, M.S., Choi, J., Kim, H., Scanlon, A. and Lee, Y.H. "Concrete beams with fiber-reinforced polymer shear reinforcement", *ACI Structural Journal*, **111**(4), pp. 903-912 (2014).
10. ACI Committee 318-11. *Building Code Requirements for Reinforced Concrete and Commentary (ACI318-11)*, p. 387, American Concrete Institute, Farmington Hills, USA (2011).
11. CSA A23.3, *Design of Concrete Structures for Buildings (CSA A23.3-04)*, p. 214, Canadian Standards Association, Mississauga, ON, Canada (2004).

Biographies

Min Sook Kim received her PhD degree from Kyung Hee University, Korea, where she is currently a Research Fellow in the Department of Architectural Engineering. Her research interests include the behavior of fiber reinforced polymer, reinforced concrete members, and the serviceability of reinforced concrete members.

Heecheul Kim received his PhD degree from New Mexico State University, NM, USA, and is currently Professor in the Department of Architectural Engineering at Kyung Hee University, Korea. His research interests include the behavior of reinforced concrete and fiber-reinforced structures for earthquake resistance.

Haeun Park received her BS degree from Kyung Hee University, Korea, where she is currently a Graduate Research Assistant in the Department of Architectural Engineering. Her research interests include the behavior of fiber reinforced polymer, reinforced concrete members, and the serviceability of prestressed concrete members.

Namshik Ahn received his PhD degree from the University of Texas at Austin, USA, and is currently Professor in the Department of Architectural Engineering at Sejong University, Korea. His research interests include polymer concrete for repair and the behavior of fiber reinforced polymer reinforced concrete members.

Young Hak Lee received his PhD degree from Pennsylvania State University, PA, USA, and is currently Associate Professor in the Department of Architectural Engineering at Kyung Hee University, Korea. His research interests include the behavior of fiber reinforced polymer, reinforced concrete members and developing analytical models of concrete structures.